Applied Surface Science 513 (2020) 145780

Contents lists available at ScienceDirect

Applied Surface Science

journal homepage: www.elsevier.com/locate/apsusc

Full Length Article

Effects of anodizing conditions and the addition of Al_2O_3/PTFE particles on the microstructure and the mechanical properties of porous anodic coatings on the AA1050 aluminium alloy

Michaela Remešová[a,*], Serhii Tkachenko[a], Daniel Kvarda[b], Ivana Ročňáková[a], Bernhard Gollas[c], Melita Menelaou[a], Ladislav Čelko[a], Jozef Kaiser[a]

[a] CEITEC – Central European Institute of Technology, Brno University of Technology, Purkyňova 123, 612 00 Brno, Czech Republic
[b] Faculty of Mechanical Engineering, Brno University of Technology, Technická 2896/2, 616 69 Brno, Czech Republic
[c] Institute for Chemistry and Technology of Materials, Graz University of Technology, Stremayrgasse 9, 8010 Graz, Austria

ARTICLE INFO

Keywords:
Anodizing
AA1050
Coating microstructure
Hillocks
Wear

ABSTRACT

In the present study, porous anodic aluminium oxide (AAO) coatings with and without particles of Al_2O_3 (aluminium oxide) and polytetrafluorethylene (PTFE) were produced on AA1050 aluminium alloy via galvanostatic anodizing in acidic electrolyte. The effects of anodizing conditions (i.e. temperature, current density and composition of electrolyte) on the morphology, thickness, and microhardness were studied via scanning electron microscopy (SEM) equipped with energy dispersive X-ray spectroscopy (EDX) and Vickers hardness tester. The results showed that the decrease of electrolyte temperature from 24 to 10 °C and the addition of 20 g/L oxalic acid to 15% H_2SO_4 electrolyte led to the formation of thicker (34 μm) and harder porous AAO coating with hillocks. Furthermore, the decrease of applied current density from 3 to 1 A/dm^2 resulted in the formation of thinner coating (10 μm) without hillocks. The intermetallic phases based on Al-Fe and Al-Fe-Si compounds present in AA1050 alloy were not preferably dissoluted during the anodizing process at 10 °C of electrolyte. The tribological properties of the anodic coatings were investigated by the dry friction test. The results showed that the addition of Al_2O_3 and PTFE particles to sulfuric-oxalic acid electrolyte resulted in hard anodic composite coatings with enhanced wear resistance.

1. Introduction

Aluminium (Al) and its alloys have been widely used in automotive, aerospace, transportation, marine, and consumer industries due to a remarkable combination of high strength-to-weight ratio, good thermal and electrical conductivities, and excellent fabrication characteristics. However, the relatively low hardness and wear resistance of pure Al and its alloys together with their high friction coefficients hinder their wider use in most engineering applications. To overcome these drawbacks and prolong the service life of components, a multitude of surface engineering approaches has been explored in order to prepare surface coatings with sufficiently enhanced mechanical and tribological properties [1].

Anodizing is one of the most widespread industrial and cost-effective methods focused on the production of decorative, durable, corrosion and wear-resistant coatings. Anodic aluminium oxide (AAO) coatings are formed during the electrochemical process when aluminium converts into its oxide under suitable anodizing conditions, such as optimal current density or voltage, type (oxalic, sulphuric, boric acid, etc.), concentration and temperature of electrolyte [1,2]. The AAO coatings are used to improve the chemical, mechanical and tribological properties of aluminium and its alloys and to increase paint adhesion before the dyeing process. In principle, two types of AAO coatings can be produced, depending on the type of electrolyte; namely, (i) a so-called barrier coating with compact microstructure, and (ii) a porous coating [2,3,4]. The compact non-porous, barrier-type AAO coatings are originated in neutral electrolytes such as borate, citrate, and phosphate solutions, and are commercially used in the field of dielectric capacitors [3,5,6].

In contrast, the porous type AAO coatings can be obtained in many other strongly acidic electrolytes, such as sulfuric, oxalic, and phosphoric acid [7,8]. Their microstructure consists of arrays of hexagonally arranged parallel nanopores. Due to their extensive customization capabilities in terms of the coating thickness, the pore diameter, and the

* Corresponding author.
E-mail address: michaela.remesova@ceitec.vutbr.cz (M. Remešová).

https://doi.org/10.1016/j.apsusc.2020.145780
Received 22 August 2019; Received in revised form 12 February 2020; Accepted 13 February 2020
Available online 15 February 2020
0169-4332/

interpore distance, these coatings have an important potential to act as templates for synthesizing various functional nanostructures and as excellent platform materials for the development of advanced devices for chemical sensing, biosensors, catalysis, energy storage, molecular filters, etc. [3,7,9,10,11].

The available literature presents numerous data on the anodizing of various commercial aluminium alloys in different electrolytes and at different combinations of anodizing process conditions. However, anodizing of alloys with a high content of alloying elements, such as Si, Fe, Mg, Mn, or Cu, is not a trivial task, since the intermetallic phases of these elements present on the surface strongly affect the formation of porous AAO coatings [12,13]. Incorporation of intermetallic phases into the AAO coating during the anodizing process results in an increase in the coating porosity and the appearance of defects, such as cracks or voids [12,13,14]. Therefore, the anodizing of commercially available technical aluminium alloys with a lower amount of intermetallic phases, such as 1070, 1050, 1100 or 3003, still has an increased practical significance.

The aluminium alloy AA1050 is of great commercial interest for anodization purposes due to its homogeneous microstructure with a low content of intermetallic compounds. Several studies on several specific aspects of the anodization of AA1050 have been reported [15,16,17,18], most of them being focused on establishing the effect of individual factors (such as electrolyte composition, concentration, temperature, and current density) or their combinations on the microstructure and mechanical properties of the obtained AAO coatings. The influence of the electrolyte type, which has already been described [16,19], is that the AAO coatings on AA1050 prepared in the mixture of sulfuric (H_2SO_4) acid and oxalic ($C_2H_2O_4$) acid electrolyte shows better densification and higher microhardness in comparison with those prepared in H_2SO_4-based electrolyte only. In addition, the electrolyte temperature demonstrates another significant impact on the resulting porosity of the AAO coatings since it shows the decreasing tendency upon decreasing the electrolyte temperature, thus, leading to a higher coating hardness [15,16,20]. Moreover, the effect of current density was investigated by Guezmil et al. [16] and Bensalah et al. [20], who both reported improvements of the AAO coating hardness and elastic modulus with increasing current density. Roshani et al. [21] reported that by using pulsed current instead of direct current, there was a positive effect of reduced porosity and increased thickness and hardness of porous AAO coatings. These improvements of the compactness and hardness of the AAO coatings resulted in a decrease in the coefficient of friction and an increase in wear resistance [16]. In summary, the most important conditions of AA1050 anodizing process were investigated to some extent. However, conducting a direct comparative analysis of these data is rather difficult due to significant differences in the sample preparation techniques and anodizing conditions reported in the literature. Therefore, a holistic picture of the effect of various anodizing conditions on the modification of microstructure and mechanical properties of AA1050 has yet to be constructed.

In addition to changing the anodizing conditions, the mechanical properties (hardness, elastic modulus, wear resistance, friction behaviour) of anodic coatings prepared on Al, Mg or Ti alloys can be further improved by forming a composite coating via embedding hard particles (such as Al_2O_3, SiC, or TiO_2) dispersed in the electrolyte or by producing a low-friction and self-lubrication coating via embedding of polytetrafluoroethylene (PTFE) particles [22,23,24,25,26]. Nevertheless, to the best of our knowledge, there are no studies dealing with the preparation of composite AAO coatings on AA1050 by incorporating Al_2O_3 particles. The incorporation of PTFE particles inside the pores and onto the surface of a porous AAO coatings on AA1050 in order to improve the tribological properties has been attempted via sedimentation technique [27], electrophoretic deposition of PTFE particles [28], hot dipping or ultrasonic impregnation in latex PTFE with subsequent heat treatment [29]. However, these techniques represent an additional technological step and do not always ensure uniform distribution of PTFE particles within the porous coating structure. In contrast, from both technological and economic point of view, the incorporation of particles into AAO coating on AA1050 substrate directly from a solution during anodization appears to be a promising direction, although the detailed studies of this process is apparently not available in the literature.

In this contribution, we present an original study of the effect of specific anodizing conditions, including the chemical composition and temperature of the electrolyte, and the current density, and the incorporation of Al_2O_3 and PTFE particles into AAO coating directly from the electrolyte. The resulting morphology, thickness, microhardness, wear resistance, and friction coefficient of porous AAO coatings on polished and chemically pre-treated AA1050 substrates were studied in detail. The results reveal that the addition of the combination of Al_2O_3 and PTFE particles can increase the hardness and improve the wear resistance and friction properties of the produced coatings. Special attention has been paid to the microstructural examination of the produced AAO coatings as well as to establish a relationship between microstructural parameters and the resulting mechanical properties.

2. Experimental

2.1. Materials

A commercially pure 1050 aluminium alloy (AA1050) sheet was cut into 50 mm × 60 mm × 6 mm samples to use them as working electrodes (anodes) in all the experiments. The chemical composition of the alloy was determined with an optical spectrometer Q4 Tasman (Bruker, Germany), showing 0.1 Si, 0.3 Fe, 0.004 Cu, 0.005 Zn, 0.008 Mg, 0.01 Ti, and Al balance wt%. The samples were ground with #800, #1200, #2000 and #4000 grit SiC papers, and further mechanically polished with 3 and 1 μm diamond paste using ethanol as the lubricant to obtain a mirror-like surface.

Analytical grade 98% sodium hydroxide (NaOH, Lach-Ner), 65% nitric acid (HNO_3, Lach-Ner), 95% sulfuric acid (H_2SO_4, Lach-Ner), 99% glycerol ($C_3H_8O_3$, Lach-Ner), 99% oxalic acid ($C_2H_2O_4$, Lach-Ner), 60 wt% PTFE dispersion in H_2O (Sigma Aldrich) and technical grade 98.5% sodium dodecylbenzenesulfonate ($CH_3(CH_2)_{11}C_6H_4SO_3Na$, SDBS, Sigma Aldrich), were used in the experiments.

2.2. Pre-treatment

Prior to the anodization, all samples were chemically pre-treated using a three-step process. Firstly, they were ultrasonically degreased in acetone, ethanol, and isopropyl alcohol for 120 s in each solution. In the second step, they were etched in 10% NaOH solution at 35 °C for 30 s, and finally, all samples were neutralized in 1:1 mixture of concentrated HNO_3 and H_2O at room temperature for 60 s. The samples were rinsed with deionised water after each pre-treatment step.

2.3. Anodizing process

The anodizing process was performed in 15% H_2SO_4 electrolyte under the variation of three process parameters; namely, the (i) anodizing temperature (24 and 10 °C), (ii) current density (1 and 3 A/dm^2), and the (iii) chemical composition of the electrolyte (including oxalic acid, and Al_2O_3 and PTFE particles). The anodizing conditions were chosen based on our preliminary results and are summarized in Table 1. In all experiments in which the lower electrolyte temperature (10 °C) was used, glycerol was added to the electrolyte to reduce the heat produced during the reactions at the oxide-substrate interface and to keep the process temperature constant [30]. A direct current (DC) power supply QPX 1200 (Aim–TTi, United Kingdom) with two stainless steel (AISI 316L) plates of dimension 50 mm × 60 mm × 2 mm as cathodes was used for anodizing. The distance between anode and cathode was 65 mm. During the anodizing process, voltage versus

Table 1
Summary of the experimental conditions.

Sample	Electrolyte	Addition of particles	Bath temperature (°C)	Current density (A/dm^2)	Anodizing time (s)
1	15% H_2SO_4*	–	24	3	1800
2	15% H_2SO_4 + 10 mL/L $C_3H_8O_3$$^{\times}$	–	10	3	1800
3	15% H_2SO_4 + 20 g/L $C_2H_2O_4$$^{\#}$ + 10 mL/L $C_3H_8O_3$	–	10	3	1800
4	15% H_2SO_4 + 20 g/L $C_2H_2O_4$ + 10 mL/L $C_3H_8O_3$	–	10	1	1800
5	15% H_2SO_4 + 20 g/L $C_2H_2O_4$ + 10 mL/L $C_3H_8O_3$	–	10	1	3600
6	15% H_2SO_4 + 20 g/L $C_2H_2O_4$ + 10 mL/L $C_3H_8O_3$	0.6 g/L SDBS$^{\circ}$ + 6 g/L Al_2O_3 + 15 mL/L 60 wt% PTFE$^{\$}$	10	3	1800
7	15% H_2SO_4 + 20 g/L $C_2H_2O_4$ + 10 mL/L $C_3H_8O_3$	0.6 g/L SDBS + 6 g/L Al_2O_3 + 15 mL/L 60 wt% PTFE	10	1	3600

H_2SO_4* - sulfuric acid; $C_3H_8O_3$$^{\times}$ - glycerol; $C_2H_2O_4$$^{\#}$ - oxalic acid; $CH_3(CH_2)_{11}C_6H_4SO_3Na$ - SDBS$^{\circ}$ - sodium dodecylbenzenesulfonate; PTFE$^{\$}$ - polytetrafluoroethylene.

anodizing time was recorded at the time interval of 1 s. The electrolyte was agitated by compressed air to ensure a uniform temperature distribution on the sample surface and in the electrolyte bath. The electrolyte was cooled with a water-glycol chillers EuroCold and its temperature was monitored with a digital thermometer. A schematic illustration of the set-up of the cell used for the experimental procedure is shown in Fig. A.1 (Supplementary Material). After anodizing, the samples were washed in deionised water and dried with cold air.

2.3.1. Preparation of stable electrolyte containing both Al_2O_3 and PTFE particles

The stable dispersion electrolyte was prepared following the protocol below:

- Solution 1: 0.6 g/L of sodium dodecylbenzenesulfonate (SDBS) was added to 5 mL of deionised water and stirred for 30 min;
- Solution 2: 6 g/L of Al_2O_3 particles (diameter < 500 nm) were added to Solution 1, and the dispersion was stirred for 60 min in an ultrasonic bath;
- Solution 3: Solution 2 was then added to 1 L of 15% H_2SO_4 containing 20 g/L of oxalic acid and 10 mL/L of glycerol, and stirred for 30 min;
- Final electrolyte: 15 mL/L of 60 wt% commercially available suspension PTFE was added to Solution 3 and kept under stirring for 12 h.

2.4. Characterization techniques

The surface morphology and cross-section of the anodic coatings were examined with a scanning electron microscope (SEM, Lyra3, Tescan, Czech Republic) equipped with X-ray energy dispersive spectroscopy (EDX, XFlash 5010, Bruker AXS Microanalysis, Germany) for chemical analyses. The surface morphology examination was carried out in both secondary electron (SE) and back-scattered electron (BSE) modes using an acceleration beam voltage of 10 keV. Samples for cross-sectional microstructure investigations were prepared by means of cold mounting technique followed by conventional metallographic procedures using an automatic grinding/polishing machine (Tegramin, Struers, Denmark). Samples were wet ground with #800-4000 SiC papers, polished with 3 and 1 μm diamond pastes and finally polished with colloidal silica suspension (OPS, Struers). Prior to the microstructural observations, the samples were coated with a 10 nm thick carbon layer using an evaporation coating unit (EM ACE600, Leica, Germany). As-coated samples cross-sections were analysed in BSE mode and by EDX for chemical analysis at an acceleration beam voltage of 10 keV.

The average coatings thickness was measured on recorded cross-sectional SEM micrograph using Olympus Stream Image Analyses Software from twenty randomly selected positions on each sample.

The microhardness of non-treated AA1050 substrate and of the porous anodic coatings was measured on the sample cross-sections by means of a Vickers hardness tester (Duramin 100, Struers, Denmark) under a constant load of 0.49 N (HV0.05) and 0.0245 N (HV0.025), and testing time of 10 s. The reported microhardness values represent the average value among 10 measurements.

The tribological behaviour of the anodic coatings at room temperature was evaluated by means of reciprocal ball-on-disc wear test using a standard tribometer UMT TriboLab (Bruker Corporation, USA) that allows recording the friction coefficient (COF) directly throughout the experiment. The counterparts were AISI G133 alumina (Al_2O_3) balls of 6 mm in diameter, which were stationary fixed in the holder and pressed to the moving coating sample by a normal load of 3 N. Alumina was chosen as the counterpart material, since it possesses high hardness and chemical inertness and is commonly used for this type of tribological evaluation of materials [31]. The sample was moving back-and-forth along a stroke of 10 mm with a frequency of 3 Hz. The duration of

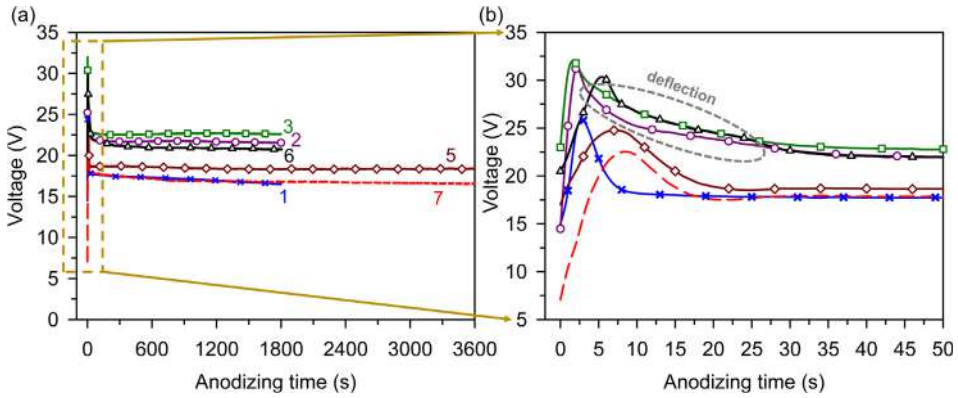

Fig. 1. Voltage vs anodizing time curves for samples 1–7 recorded during anodizing of AA1050 at different process conditions (a) after 3600 s and (b) detail of the record up to 50 s.

the test was 2000 cycles. After the test, the cross-sectional profiles of wear tracks were measured with an optical profiler Contour GT X8 (Bruker Corporation, USA), and the total wear loss of the samples was calculated as a resulting cross-sectional area of the wear track multiplied by its length.

3. Results and discussion

3.1. Anodizing process

Fig. 1 shows the voltage vs anodizing time curves for AA1050 recorded during the anodizing process. These curves are commonly used for identifying the formation of porous types of AAO coatings during galvanostatic anodizing of aluminium and its alloys in sulfuric, phosphoric, or oxalic acid [32,33]. In all cases, the measured data revealed the development of AAO coatings starting with the formation of a compact (barrier) type of anodic oxide coating evidenced by the linear increase of the voltage at the beginning of the anodization process. As the local maximum of voltage is reached, the anodizing process continues with the breakdown of the tight compact AAO coating, with pore nucleation, and with the formation of a porous structure. Finally, a voltage plateau is reached as a result of the steady-state growth of porous AAO coatings [3]. The variation of anodizing parameters, such as temperature, current density, and chemical composition of the electrolyte, strongly influenced the slope of the voltage vs anodizing time curves (samples 1–7), which is related to the growth rate and thickness of the barrier and porous types of AAO coatings.

A decrease of the anodizing temperature from 24 °C (curve 1) down to 10 °C (curve 2), while keeping a constant current density of 3 A/dm^2, resulted in an increase of the voltage and the formation of thicker coatings with smaller pores, as shown in detail later in Section 3.2.

Addition of 20 g/L of oxalic acid to the 15% H_2SO_4 electrolyte (curve 3) led to a slight increase of the voltage in comparison to the process without oxalic acid (curve 2). This indicates an increase in the growth rate of the barrier type AAO coating. The presence of oxalic acid reduces oxide dissolution and leads to the formation of less porous and more compact AAO coatings [34]. At the same time, a lower current density of 1 A/dm^2 (curves 5 and 7) results in lower voltages in comparison with the anodization at higher current densities (curves 1–3, 6). This indicates lower oxygen, hydroxide, and sulfur ions migration rate and, as a result, a decrease in barrier coating thickness [32,35].

Addition of Al_2O_3 and PTFE particles to the electrolyte (curves 6 and 7) also led to a decrease of the voltage in comparison with the experiments without particles (curves 3 and 5). Moreover, the time required to reach the maximum voltage is longer for the particle-containing electrolyte (Fig. 1a), which suggests a small growth rate of the porous anodic coating.

Interestingly, some deflection from a continuous descent of the slope was detected during the anodizing processes with higher current density and lower temperature of the electrolyte (this deflection is highlighted in curves 2, 3, and 6 in the inset of Fig. 1a). This type of deflection in the voltage vs anodizing time curves was also observed by Aerts et al. [36] and is attributed to a local burning of electrolyte at the sample surface during the anodizing process.

3.2. Topography and microstructure of anodic coatings

3.2.1. Surface morphology prior to anodizing

Scanning electron micrographs (secondary electrons) of the initial polished substrates surface before and after chemical pre-treatment are shown in Fig. 2. The surface of polished samples before chemical pre-treatment was smooth with only a small number of scratches produced during mechanical polishing and featureless intermetallic phases. EDX analysis revealed that intermetallic phases present in AA1050 are most

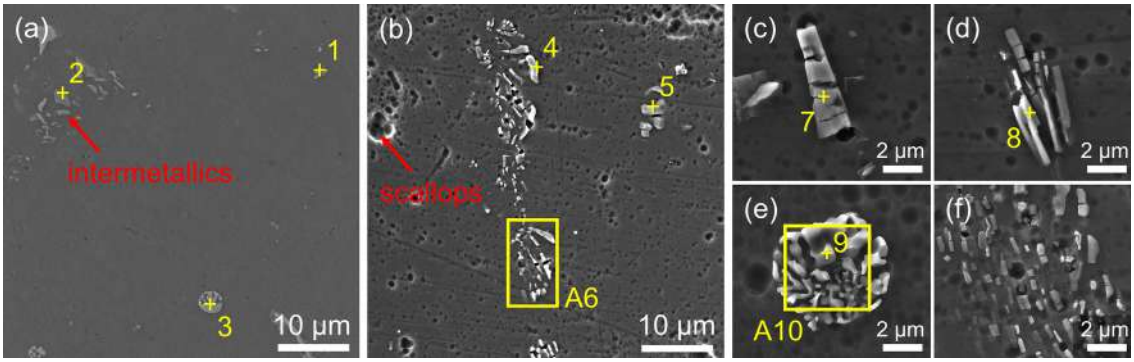

Fig. 2. Micrographs (SEM-SE) of initial surface topography of the AA1050 alloy after (a) polishing, (b-f) chemical pre-treatment, and (c-f) detail of intermetallic phases morphology.

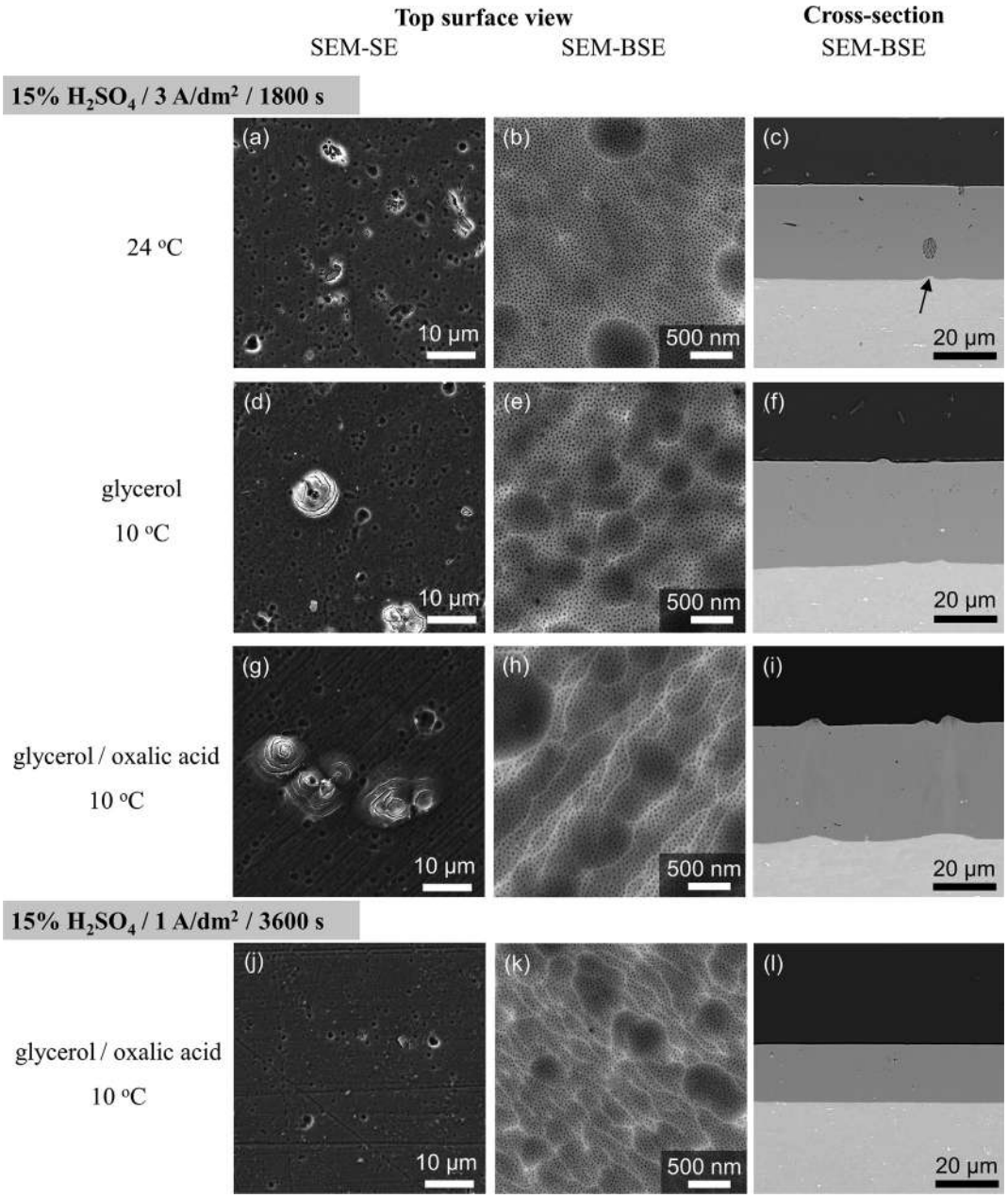

Fig. 3. Micrographs of the top view (left and middle) and cross-section (right) after anodizing under the influence of: (i) current density (a–i) 3 A/dm^2, (j–l) 1 A/dm^2, (ii) temperature (a–c) 24 °C, (d–l) 10 °C and (iii) composition of electrolyte (a–c) 15% H_2SO_4, (d–f) 15% H_2SO_4 + 10 mL/L glycerol, (g–l) 15% H_2SO_4 + 20 g/L oxalic acid + 10 mL/L glycerol on the morphology and thickness of porous AAO coatings.

often based on Al-Fe and Al-Fe-Si compounds, as shown in Table A.1 (Supplementary Material). As can also be seen from Table A.1 (Supplementary Material), the round-shaped particles contain more Si in comparison with the irregular-shaped ones. Particles with such morphology were previously observed [12,18]. After chemical pre-treatment, the intermetallic phases were clearly visible on scalloped surface, because the rate of aluminium matrix dissolution in NaOH was higher than the dissolution rate of iron and silicon [37,38].

3.2.2. Effect of anodization temperature, electrolyte composition, and current density on the porous coating microstructure and thickness

Fig. 3,4 and A.2 (Supplementary Material) depict the effect of different anodizing parameters, such as temperature, electrolyte composition, and current density, on the morphology and resulting thickness of the porous AAO coatings produced at AA1050 alloy substrates. The surface morphology of coating #1 produced at 24 °C in 15% H_2SO_4 at 3 A/dm^2 (Fig. 3a and Fig. 4a–b) shows cavities, whose shapes and dimensions are similar to those of the intermetallic phases observed on the chemically pre-treated surface of the substrate alloy. The presence of cavities can be explained by the preferred dissolution of those intermetallic phases during the anodizing process in the H_2SO_4 electrolyte [13,14]. The thickness of the porous AAO coating was 30 µm.

Intermetallic phases based on Al-Fe and Al-Fe-Si have lower oxidation rates than the aluminium matrix and, therefore, can be trapped in the coating during the anodizing process, thus reducing the local growth of the porous AAO coating [39]. This phenomenon can be confirmed at the coating cross-section (Fig. 3c, marked with an arrow), where decrease in thickness can be seen under the round-shaped intermetallic phase. The chemical composition analysis (Fig. 4 and Table A.3, Supplementary Material) showed a significantly lower Fe content in the intermetallic phase that confirmed a higher dissolution rate of Fe compare to Si during the anodic oxidation process. Location of the

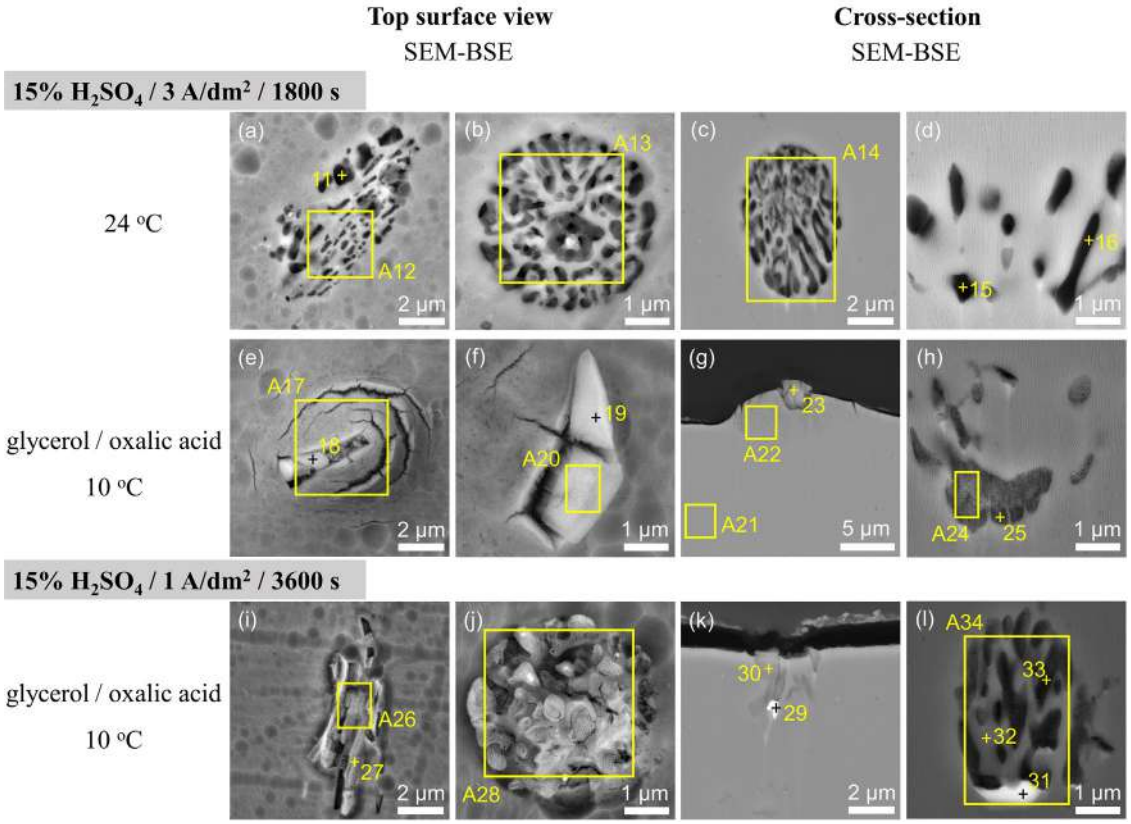

Fig. 4. Micrographs of intermetallic phases after anodizing under: (i) temperatures of (a–d) 24 °C, (e–l) 10 °C, (ii) current densities of (a–h) 3 A/dm^2, (i–l) 1 A/dm^2 and (iii) electrolyte composition of (a–d) 15% H_2SO_4, (e–l) 15% H_2SO_4 + 20 g/L oxalic acid + 10 mL/L glycerol.

intermetallic phase, the increased oxygen content was registered, promoting its partial oxidation.

When lower electrolyte temperature was used (10 °C) at the same current density (3 A/dm^2), a thicker coating (33 µm) with hillocks and cracks was produced (Fig. 3d–f). The difference in anodizing behaviour under the reduction of anodizing temperature from 24 down to 10 °C was clearly observed at the voltage vs anodizing time curves (Fig. 1a, marked as deflection) that is related to what is known as the burning phenomenon. This phenomenon is associated with high local anodic current densities and corresponding local temperature bursts, possibly at the sites of intermetallic particles, and is responsible for the formation of hillocks in the sulfuric acid electrolyte observed by other researchers as well [32,33,36]. Hard anodizing conditions, involving low electrolyte temperatures and high current densities, are prone to burn and therefore to hillock appearance.

The cracks were predominantly observed around hillocks and intermetallic phases (Fig. 4e–g). The cracks observed around hillocks are attributed to high mechanical stress accompanied by a high local current density and a fast growth of the AAO coating at the site of the hillocks [36]. The formation of cracks around the intermetallic phases is predominantly caused by an increase in the volume of the oxidized intermetallic particles. The intermetallic phases were oxidized faster than when anodizing at a lower current density, in which case the local cracks on the surface were not detected.

The addition of oxalic acid (20 g/L) to the electrolyte, led to the formation of thicker coatings (34 µm) with typical morphology and formation of hillocks (Fig. 3h and 3g). When the current density was changed to 1 A/dm^2, significantly thinner coatings were formed but without hillocks and local cracks at the coating surface, as shown in Fig. 3j-l. With increasing anodizing time, from 1800 s to 3600 s, the thickness of the coating increased from 10 to 19 µm.

The EDX analysis showed the presence of aluminium, oxygen and sulfur at the porous AAO coatings. However, some differences in the chemical composition were detected (Table A.2, Supplementary Material). The porous AAO coatings produced at a higher current density and at the lower temperature contained more sulfur and less aluminium. These findings are in agreement with observations made by Gastón-García et al. [32]. Detailed SEM and EDX investigation of hillocks on the surface and at the cross-section (Fig. 4e, i and Table A.3, Supplementary Material), revealed that the hillocks contained more sulfur and oxygen than the surrounding AAO coating. Iron and silicon were detected on the top of the hillocks. Gastón-García et al. [32] suggested that the presence of intermetallic Fe and Si-based phases in the aluminium alloy initiate local burning, which promotes the formation of hillocks. Moreover, Michalska-Domanska et al. [10] observed hillocks on the surface of oxide coatings formed on both low and high purity aluminium, suggesting that their formation is associated with the incorporation of sulfate ions rather than the presence of impurities in the examined material. Thus, the behaviour of intermetallic phases located in the base material after anodizing and the hillocks were studied in detail (Fig. 4). It was found that the electrolyte temperature has a notable effect on the oxidation/dissolution of intermetallic phases. When the higher electrolyte temperature of 24 °C was used, the intermetallic phases on the surface were preferably dissolved (Fig. 4a–b). This was distinct from anodization at the lower electrolyte temperature of 10 °C, in which case the intermetallic phases on the surface were oxidized (Fig. 4f–h). The EDX analysis of each area of the phases present in Fig. 4 is given in Table A.3 (Supplementary Material). As can be seen, samples produced at higher electrolyte temperature contained lower amount of Fe and Si in comparison with the samples produced at low temperature, which contained more oxygen.

3.2.3. *Microstructure and thickness of anodic composite coatings*

Surface morphologies and cross-sections of the anodic composite

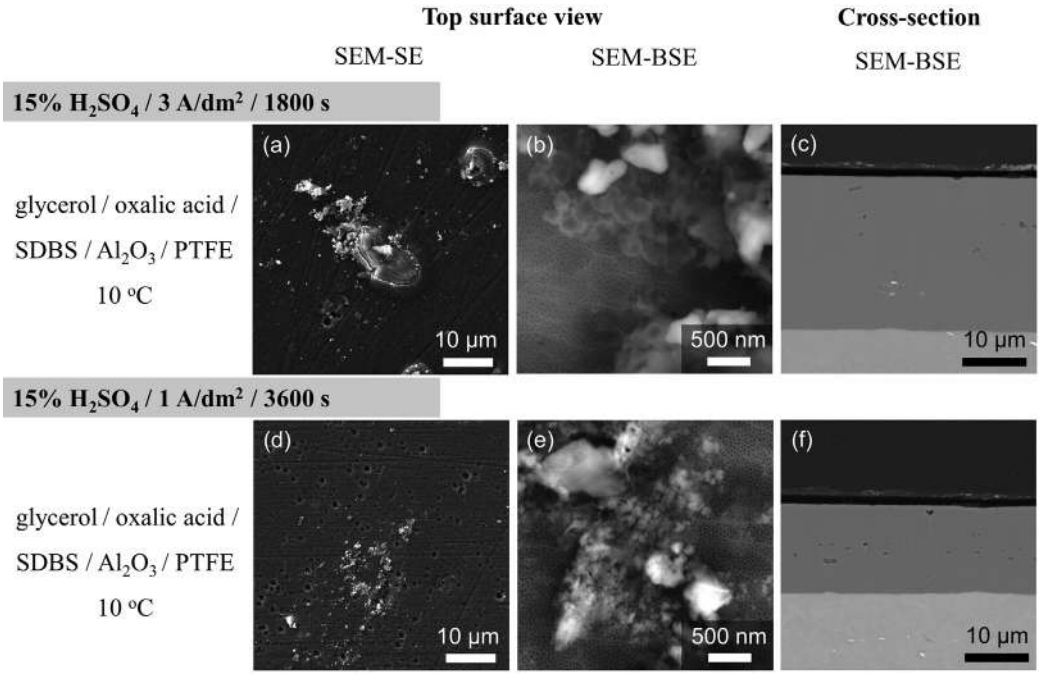

Fig. 5. Micrographs of anodic composite coatings produced under different current densities and anodizing times (a–c) 3 A/dm^2 and 1800 s, (d–f) 1 A/dm^2 and 3600 s.

coatings prepared from a dispersion electrolyte which contained 6 g/L of Al_2O_3 and 15 mL/L of 60 wt% PTFE anodized at 3 A/dm^2 for 1800 s and at 1 A/dm^2 for 3600 s, respectively, are shown in Fig. 5a–d and Fig. 5e–h. No significant differences in the surface morphology between the AAO coatings (Fig. 3g, h and Fig. 3j, k) and the anodic composite coatings (Fig. 5a–c, Fig. 5e–g) were observed, irrespective of the addition of Al_2O_3 and PTFE particles. Al_2O_3 and PTFE particles on the coating surface were non-uniformly distributed, as can be seen in Fig. 5e.

Fig. 3i and 3l show the cross-sectional SEM micrographs of the anodic coatings formed in the electrolyte without particles, while Fig. 5d and 5h show the cross-sectional SEM micrographs with particles. It is evident that the particle-free AAO coatings (34 and 19 μm) are thicker than the coatings with inserted particles (24 and 14 μm). This phenomenon is correlated to the anodizing voltage (Fig. 1), which was found to be lower for the sample anodized in the electrolyte which contained the particles.

3.3. Microhardness, friction coefficients, and wear loss

Microhardness measurements (Fig. 6a) showed that all anodic coatings were 10–12 times harder than the substrate alloy. Decrease in the electrolyte temperature, from 24 down to 10 °C, increased the coating hardness, from 400 to 470 kg/mm^2. This is consistent with earlier studies reported in the literature [16,40], which correlated the hardness increase with the improvement of the coating compactness. It has been shown in the literature [40,41,42] that the dissolution rate at the oxide/electrolyte interface is lower at the lower anodizing temperature, especially on the top of pores and pore-walls, which resulted in the formation of less porous AAO coatings [40,41,42]. A further increase in hardness was observed for coating #3, which was prepared in the oxalic acid electrolyte. This is due to the densification of the anodic coating and the decrease in the coating porosity [16,42,43]. Furthermore, an increase in hardness was also achieved for coating #6 through the addition of Al_2O_3 and PTFE particles to the electrolyte. Harder polycrystalline alumina particles entrapped in the slightly softer AAO coating with amorphous alumina microstructure improved its hardness. The presence of PTFE particles, on the other hand, reduced the formation of pores and decreased the size of the pores, which is consistent with observations by Chen et al. [22]. It should be noted that the hardness values obtained in this study for the composite anodic coatings (~510 to 520 kg/mm^2), were found substantially higher than those obtained by Chen et al. [22] and it can be explained by the difference in the applied anodizing conditions.

An important observation was that the AAO coatings #2, #3, and the composite anodic coating #6 exhibited a high data scatter of microhardness due to the presence of a high number of hillocks on the surface, as shown in Fig. 3d, g, and Fig. 5a. Roa et al. [44] studied in detail the mechanical properties of porous AAO coating containing hillocks and confirmed by nanohardness measurements that the hillocks have locally lower hardness due to higher porosity. Higher microstructural homogeneity with fewer hillocks was obtained by lowering the current density from 3 to 1 A/dm^2 (Figs. 3j, 5e), which also provided a more uniform hardness distribution across the coatings #5 and #7. This was accompanied by only a slight decrease in hardness when compared with the coatings #4 and #6 that were prepared with 3 A/dm^2. The most uniform anodic coating morphology with the lowest number of hillocks, high and uniform hardness was achieved in the anodic composite coating #7 by applying a combination of low anodizing temperature, low anodic current density, and addition of both Al_2O_3 and PTFE particles.

Tribological tests showed that the anodic oxide coatings have a much lower coefficient of friction (COF) in comparison with the substrate alloy without anodization (Fig. 6b). No significant effect of any anodizing parameter on the COF of the anodic coatings was observed. Similarly, the addition of Al_2O_3 and PTFE particles to the electrolyte did not produce any significant change in the COF for the anodic composite coating #6. This differs from earlier studies on the modification of anodic composite coatings by post-treatment sedimentation technique in PTFE dispersion solution [27], where a significant reduction of the COF was observed. This behaviour can be explained by the low amount and uneven distribution of particles in the composite anodic coating produced in this study, which seems insufficient for the formation of a stable self-lubricating coating. Thus, the contact of the counterpart is

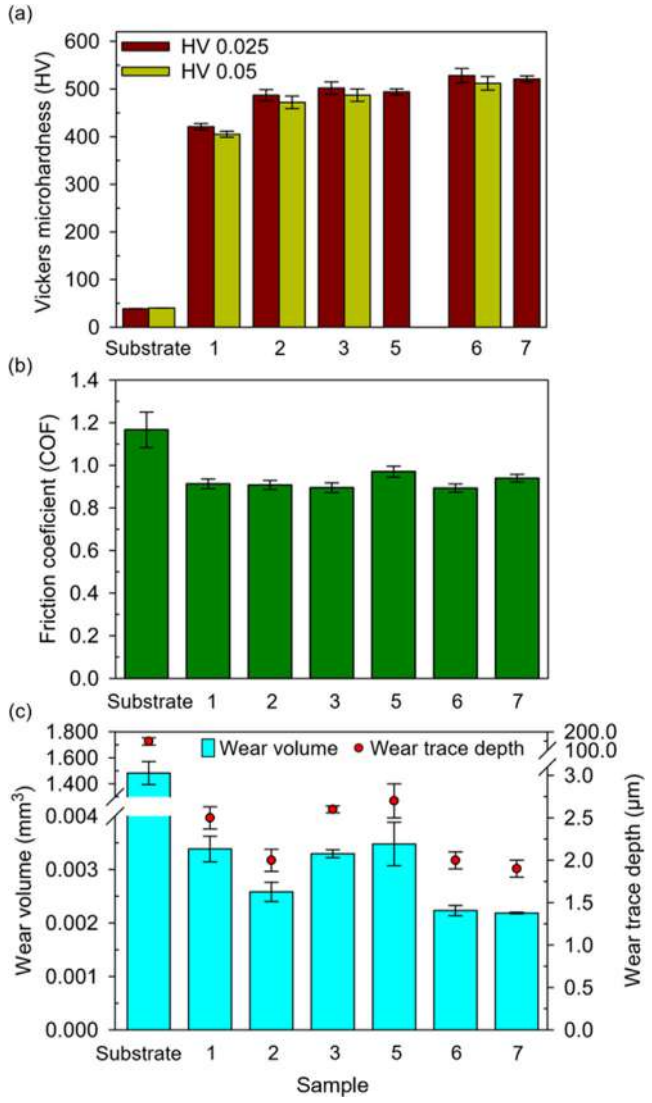

Fig. 6. (a) Microhardness, (b) friction coefficient and (c) wear volume along with the depth of wear tracks for the produced anodic coatings (1 to 7).

accomplished on the porous coating surface rather than on the PTFE thin film. At the same time, a decrease of current density from 3 to 1 A/dm^2 led to a distinct increase of the COF in the coatings #5 and #7. The reason for this might be the difference in pore size and morphology, anion-contamination of the anodic coatings, and higher internal stresses as, compared to the rest of the examined coatings. However, the explanation of this behaviour requires deeper investigations.

The analysis of the wear loss revealed two orders of magnitude higher wear resistance among the anodic coatings and the substrate. During the wear test, the substrate was not exposed, as can be observed from the results on wear trace depth measurements (Fig. 6c), where the wear loss clearly occurred at the expense of only the AAO coating. The reduction in wear loss of the coating #2 occurred due to its specific microstructure formed at a decreased anodization temperature when compared to the coating #1, while the coatings obtained with the further addition of oxalic acid and at reduced current density showed lower wear resistance. The improvement of wear resistance of the anodized coatings by reducing the electrolyte temperature seems to be primarily associated with a decrease in the porosity, while the higher number of defects in porous AAO coatings is related to the increase of its mechanical properties [45]. Previous data [16] also indicated that the wear resistance of the AAO coating may be influenced not only by the porosity, surface roughness, and hardness, but also by other properties, such as the shear strength and crack resistance [16]. Such conclusion is also supported by a significant reduction of the wear loss; the anodic composite coatings #6 and #7 showed the lowest loss, which was further improved by adding Al_2O_3 and PTFE particles. Despite the absence of significant effects of the particles on the friction coefficient of the porous AAO coatings, it is obvious that the presence of Al_2O_3 and PTFE particles at anodic composite coatings results in the improvements of their shear strength and elasticity. Consequently, the AAO coatings are able to sustain higher deformation under reciprocal non-lubricated sliding wear tests without any significant change. This is of critical importance for some specific applications in transportation systems, especially in the aerospace and automobile products, where the supply of lubricating additives is limited by the operating conditions.

4. Conclusions

In this study, a wide range of anodizing conditions, including electrolyte temperature and composition, current density, and the addition of Al_2O_3 and PTFE particles to the electrolyte, has been applied to aluminium alloy AA1050 substrate to produce porous anodic aluminium oxide coatings. The effect of the above-mentioned conditions on the resulting morphology, hardness and tribology properties of the porous AAO coatings were extensively and systematically examined, and the following main conclusions were drawn:

1. The porous AAO coatings were formed during galvanostatic anodizing in 15% sulfuric acid electrolyte without or with the addition of oxalic acid (20 g/L $H_2C_2O_4$), 6 g/L Al_2O_3, and 15 mL/L 60 wt% PTFE commercial suspension;
2. Decrease in the electrolyte temperature, from 24 down to 10 °C, led to the formation of thicker and harder coatings containing hillocks with local cracks. Addition of 20 g/L of oxalic acid to the electrolyte also had a possible effect on the increased thickness and hardness of produced coatings but not such as was observed in the case of decrease in the temperature of the electrolyte;
3. Improvement of the porous AAO coating quality via defect (cracks, hillocks) elimination can be achieved by decreasing the current density from 3 to 1 A/dm^2, although the thickness reduction from 34 μm to 10 μm was observed at the same time;
4. AA1050 material contains intermetallic phases based on Al-Fe and Al-Fe-Si compounds with irregular and round shape. These intermetallic phases were preferably dissolved during anodizing at 24 °C of electrolyte, and were, on the contrary, preferably oxidized in the case of anodizing at 10 °C;
5. The microstructural examination revealed the successive incorporation of Al_2O_3 and PTFE particles in the produced coatings and the resulting hardness and wear resistance was 4% and 30% higher, respectively, than those of the non-composite AAO coating obtained under the same anodizing conditions in the sulfuric-oxalic based electrolyte without particles. At the same time, friction did not improve strongly, apparently due to insufficient concentration of the PTFE in surface tribo-film;
6. The porous composite AAO coating without structural defects (hillocks and cracks) and with the best combination of mechanical properties, such as high hardness, low COF, and high wear resistance, were prepared by anodization at low temperature (10 °C) and at low current density (1 A/dm^2) in electrolyte with a dispersion of Al_2O_3 and PTFE particles.

CRediT authorship contribution statement

Michaela Remešová: Conceptualization, Methodology, Writing - original draft, Investigation. **Serhii Tkachenko:** Writing - original draft, Writing - review & editing, Formal analysis. **Daniel Kvarda:** Investigation. **Ivana Ročňáková:** Methodology, Investigation.

Bernhard Gollas: Writing - review & editing. **Melita Menelaou:** Writing - review & editing, Visualization. **Ladislav Čelko:** Supervision, Writing - review & editing. **Jozef Kaiser:** Supervision.

Declaration of Competing Interest

The authors declare that they have no known competing financial interests or personal relationships that could have appeared to influence the work reported in this paper.

Acknowledgements

This project was received funded from the Specific Research Project, CEITEC Brno University of Technology, Czech Republic (STI-J-18-5308). This work was supported by the European Social Fund (ESF) under Project CZ.02.2.69/0.0/0.0/18_070/0009469. Authors also want to acknowledge the project CEITEC 2020, Czech Republic (LQ1601) with financial support from the Ministry of Education,Youth and Sports of the Czech Republic under the National Sustainability Program II, and CEITEC Nano Research Infrastructure, Czech Republic (ID LM2015041, MEYS CR, 2016-2019) providing the access to devices used for this study.

Appendix A. Supplementary material

Supplementary data to this article can be found online at https://doi.org/10.1016/j.apsusc.2020.145780.

References

[1] J.R. Davis, ASM Speciality Handbook: Aluminium and Aluminium Alloys, ASM International, Materials Park, Ohio, 1993.
[2] H. Ding, Surface Engineering of Light Alloys Aluminium, Magnesium and Titanium Alloys, first ed., CRC Press, Boca Raton, Boston, New York, 2010.
[3] G.D. Sulka, Highly Ordered Anodic Porous Alumina Formation by Self-Organized Anodizing, A. Eftekhari (Eds.), Nanostruct. Mater. Electrochem. (2008), pp. 1-116. https://doi.org/10.1002/9783527621507.ch1.
[4] E. Ghali, Corrosion Resistance of Aluminum and Magnesium Alloys: Understanding, Performance, and Testing, John Wiley and Sons, Hoboken, New Jersey, 2010.
[5] H. Takahashi, M. Nagayama, Electrochemical behaviour and structure of anodic oxide films formed on aluminium in a neutral borate solution, Electrochim. Acta 23 (1978) 279–286, https://doi.org/10.1016/0013-4686(78)85058-0.
[6] D. Nakajima, T. Kikuchi, S. Natsui, R.O. Suzuki, Mirror-finished superhydrophobic aluminum surfaces modified by anodic alumina nanofibers and self-assembled monolayers, Appl. Surf. Sci. 440 (2018) 506–513, https://doi.org/10.1016/j.apsusc.2018.01.182.
[7] G.E.J. Poinern, N. Ali, D. Fawcett, Progress in nano-engineered anodic aluminum oxide membrane development, Mater. 4 (2011) 487–526, https://doi.org/10.3390/ma4030487.
[8] T. Kikuchi, A. Takenaga, S. Natsui, R.O. Suzuki, Advanced hard anodic alumina coatings via etidronic acid anodizing, Surf. Coat. Technol. 326 (2017) 72–78, https://doi.org/10.1016/j.surfcoat.2017.07.043.
[9] L. Zaraska, G.D. Sulka, J. Szeremeta, M. Jaskuła, Porous anodic alumina formed by anodization of aluminum alloy (AA1050) and high purity aluminum, Electrochim. Acta 55 (2010) 4377–4386, https://doi.org/10.1016/j.electacta.2009.12.054.
[10] M. Michalska-Domańska, M. Norek, W.J. Stępniowski, B. Budner, Fabrication of high quality anodic aluminum oxide (AAO) on low purity aluminum - a comparative study with the AAO produced on high purity aluminum, Electrochim. Acta 105 (2013) 424–432, https://doi.org/10.1016/j.electacta.2013.04.160.
[11] H. Zhao, L. Liu, Y. Lei, A mini review: Functional nanostructuring with perfectly-ordered anodic aluminum oxide template for energy conversion and storage, Front. Chem. Sci. Eng. 12 (2018) 481–493, https://doi.org/10.1007/s11705-018-1707-x.
[12] M. Jariyaboon, P. Møller, R.E. Dunin-Borkowski, R. Ambat, FIB-SEM investigation of trapped intermetallic particles in anodic oxide films on AA1050 aluminium, Anti-Corros. Methods Mater. 58 (2011) 173–178, https://doi.org/10.1108/00035591111148885.
[13] S. Li, Y. Li, Y. Zhang, J. Liu, M. Yu, Effect of intermetallic phases on the anodic oxidation and corrosion of 5A06 aluminum alloy, Int. J. Miner. Metall. Mater. 22 (2015) 167–174, https://doi.org/10.1007/s12613-015-1057-3.
[14] F. Snogan, C. Blanc, G. Mankowski, N. Pébère, Characterisation of sealed anodic films on 7050 T74 and 2214 T6 aluminium alloys, Surf. Coat. Technol. 154 (2002) 94–103, https://doi.org/10.1016/s0257-8972(01)01717-0.
[15] T. Aerts, T. Dimogerontakis, I. De Graeve, J. Fransaer, H. Terryn, Influence of the anodizing temperature on the porosity and the mechanical properties of the porous anodic oxide film, Surf. Coat. Technol. 201 (2007) 7310–7317, https://doi.org/10.1016/j.surfcoat.2007.01.044.
[16] M. Guezmil, W. Bensalah, A. Khalladi, K. Elleuch, M. Depetris-Wery, H.F. Ayedi, Friction coefficient and microhardness of anodized aluminum alloys under different elaboration conditions, Trans. Nonferrous Met. Soc. China English Ed. 25 (2015) 1950–1960, https://doi.org/10.1016/S1003-6326(15)63803-1.
[17] S. Hamid, B. Sohrabi, M.R. Noori, H.R.T. Bahrami, Optimal condition for fabricating superhydrophobic aluminum surfaces with controlled anodizing processes, Appl. Surf. Sci. 435 (2018) 1322–1328, https://doi.org/10.1016/j.apsusc.2017.11.188.
[18] J.M. Montero-Moreno, M. Sarret, C. Müller, Self-ordered porous alumina by two-step anodizing at constant current: behaviour and evolution of the structure, Micropor. Mesopor. Mater. 136 (2010) 68–74, https://doi.org/10.1016/j.micromeso.2010.07.022.
[19] J. Lee, Y. Kim, U. Jung, W. Chung, Thermal conductivity of anodized aluminum oxide layer: the effect of electrolyte and temperature, Mater. Chem. Phys. 141 (2013) 680–685, https://doi.org/10.1016/j.matchemphys.2013.05.058.
[20] W. Bensalah, M. DePetris-Wery, H.F. Ayedi, Young's modulus of anodic oxide layers formed on aluminum in sulphuric acid bath, Mater. Lett. 179 (2016) 82–85, https://doi.org/10.1016/j.matlet.2016.05.035.
[21] M. Roshani, A.S. Rouhaghdam, M. Aliofkhazraei, A.H. Astaraee, Optimization of mechanical properties for pulsed anodizing of aluminum: the effect of electrolyte and temperature, Surf. Coat. Technol. 310 (2017) 17–24, https://doi.org/10.1016/j.surfcoat.2016.12.046.
[22] S. Chen, C. Kang, J. Wang, C. Liu, K. Sun, Synthesis of anodizing composite films containing superfine Al_2O_3 and PTFE particles on Al alloys, Appl. Surf. Sci. 256 (2010) 6518–6525, https://doi.org/10.1016/j.apsusc.2010.04.040.
[23] J. Liang, L. Hu, J. Hao, Preparation and characterization of oxide films containing crystalline TiO_2 on magnesium alloy by plasma electrolytic oxidation, Electrochim. Acta 52 (2007) 4836–4840, https://doi.org/10.1016/j.electacta.2007.01.059.
[24] D. Zhang, Y. Gou, Y. Liu, X. Guo, A composite anodizing coating containing superfine Al_2O_3 particles on AZ31 magnesium alloy, Surf. Coat. Technol. 236 (2013) 52–57, https://doi.org/10.1016/j.surfcoat.2013.04.059.
[25] S. Li, X. Yu, J. Liu, M. Yu, L. Wu, K. Yang, Microstructure and abrasive wear behaviour of anodizing composite films containing SiC nanoparticles on Ti6Al4V alloy, J. Cent. South Univ. 21 (2014) 4415–4423, https://doi.org/10.1007/s11771-014-2443-0.
[26] M.H. Chen, K.C. Kao, M.W. Tu, D.N. Zhang, Self-Lubricating SiC/PTFE composite coating formation on surface of aluminium alloy, Adv. Mater. Res. 490–495 (2012) 3511–3515, https://doi.org/10.4028/www.scientific.net/amr.490-495.3511.
[27] J. Escobar, L. Arurault, V. Turq, C. Müller, Improvement of the tribological behavior of PTFE-anodic film composites prepared on 1050 aluminum substrate, Appl. Surf. Sci. 258 (2012) 8199–8208, https://doi.org/10.1016/j.apsusc.2012.05.022.
[28] D. Zhang, G. Dong, Y. Chen, Q. Zeng, Electrophoretic deposition of PTFE particles on porous anodic aluminum oxide film and its tribological properties: The effect of electrolyte and temperature, Appl. Surf. Sci. 290 (2014) 466–474, https://doi.org/10.1016/j.apsusc.2013.11.114.
[29] H. Wang, H. Yi, H. Wang, Q. Zeng, Analysis and self-lubricating treatment of porous anodic alumina film formed in a compound solution: The effect of electrolyte and temperature, Appl. Surf. Sci. 252 (2005) 1662–1667, https://doi.org/10.1016/j.apsusc.2005.03.141.
[30] J.M. Runge, Enhancing anodic aluminum oxide for bonding applications, Proceedings of the 24th Annual AAC Conference, San Diego, (2015).
[31] ASTM G99-95a(2000)e1, Standard test method for wear testing with a pin-on-disk apparatus, ASTM International, West Conshohocken, PA, 2000. https://doi.org/10.1520/G0099-95AR00E01.
[32] B. Gastón-García, E. García-Lecina, J.A. Díez, M. Belenguer, C. Müller, Local burning phenomena in sulfuric acid anodizing: analysis of porous anodic alumina layers on AA1050, Electrochem. Solid-State Lett. 13 (2010) C33–C35, https://doi.org/10.1149/1.3478482.
[33] P.-S. Wei, T.-S. Shih, Monitoring the progressive development of an anodized film on aluminum, J. Electrochem. Soc. 154 (2007) C678–C683, https://doi.org/10.1149/1.2780864.
[34] S.S. Abdel-Rehim, H.H. Hassan, M.A. Amin, Galvanostatic anodization of pure Al in some aqueous acid solutions Part I: Growth kinetics, composition and morphological structure of porous and barrier-type anodic alumina films, J. Appl. Electrochem. 32 (2002) 1257–1264, https://doi.org/10.1023/A:1021662814303.
[35] S. Ide, P. Mishra, K.R. Hebert, Transient relaxations of ionic conductance during growth of porous anodic alumina films: electrochemical impedance spectroscopy and current step experiments, Electrochim. Acta 222 (2016) 641–647, https://doi.org/10.1016/j.electacta.2016.11.019.
[36] T. Aerts, I. De Graeve, H. Terryn, Study of initiation and development of local burning phenomena during anodizing of aluminium under controlled convection, Electrochim. Acta 54 (2008) 270–279, https://doi.org/10.1016/j.electacta.2008.08.004.
[37] E.V. Koroleva, G.E. Thompson, G. Hollrigl, M. Bloeck, Surface morphological changes of aluminium alloys in alkaline solution: effect of second phase material, Corros. Sci. 41 (1999) 1475–1495, https://doi.org/10.1016/s0010-938x(98)00188-7.
[38] M. Witkowska, G.E. Thompson, T. Hashimoto, E. Koroleva, Assessment of the surface reactivity of AA1050 aluminium alloy, Surf. Interface Anal. 45 (2013) 1585–1589, https://doi.org/10.1002/sia.5271.
[39] A. Hakimizad, K. Raeissi, F. Ashrafizadeh, Characterization of aluminum anodized layers modified in sulfuric and phosphoric acid baths and their effect on conventional electrolytic coloring, Surf. Coat. Technol. 206 (2012) 2438–2445, https://doi.org/10.1016/j.surfcoat.2011.10.046.
[40] L.E. Fratila-Apachitei, J. Duszczyk, L. Katgerman, AlSi(Cu) anodic oxide layers formed in H_2SO_4 at low temperature using different current waveforms, Surf. Coat. Technol. 165 (2003) 232–240, https://doi.org/10.1016/S0257-8972(02)00733-8.

[41] L. Vojkuvka, A. Santos, J. Pallarès, J. Ferré-Borrull, L.F. Marsal, J.P. Celis, On the mechanical properties of nanoporous anodized alumina by nanoindentation and sliding tests, Surf. Coat. Technol. 206 (2012) 2115–2124, https://doi.org/10.1016/j.surfcoat.2011.09.040.

[42] V. Moutarlier, M.P. Gigandet, J. Pagetti, B. Normand, Influence of oxalic acid addition to chromic acid on the anodizing of Al 2024 alloy, Surf. Coat. Technol. 182 (2004) 117-123. https://doi.org/10.1016/S0257-8972(03)00875-2.

[43] M. Yoshimoto, Y. Morizono, S. Tsurekawa, T. Baba, Anodizing of aluminum in sulfuric acid and oxalic acid solutions with percarboxylic acid-based additive, J. Ceram. Soc. Japan. 120 (2012) 276–279, https://doi.org/10.2109/jcersj2.120.276.

[44] J.J. Roa, B. Gastón-García, E. García-Lecina, C. Müller, Mechanical properties at nanometric scale of alumina layers formed in sulphuric acid anodizing under burning conditions, Ceram. Int. 38 (2012) 1627–1633, https://doi.org/10.1016/j.ceramint.2011.09.053.

[45] J. Lu, G. Wei, Y. Yu, C. Guo, L. Jiang, Aluminum alloy AA2024 anodized from the mixed acid system with enhanced mechanical properties, Surf. Interfaces 13 (2018) 46–50, https://doi.org/10.1016/j.surfin.2018.08.003.